Nonlinear Dyn (2020) 100:907–919
https://doi.org/10.1007/s11071-020-05506-9

ORIGINAL PAPER

Permutation-based time irreversibility in epileptic electroencephalograms

Wenpo Yao · Jiafei Dai · Matjaž Perc · Jun Wang · Dezhong Yao · Daqing Guo

Received: 7 November 2019 / Accepted: 23 January 2020 / Published online: 4 February 2020

Abstract Time irreversibility is one of the fundamental properties of nonequilibrium complex brain activities and is relevant to various neurological conditions, e.g., epilepsy. However, the estimation of the joint probability distribution for quantitative time irreversibility (qTIR) is not trivial, and the application of qTIR in characterizing epileptic brain signals has received little attention. In this paper, we employ equal-value permutations instead of raw vectors to simplify qTIR, and we apply subtraction-based parameters to measure the probabilistic differences in order patterns for qTIR considering the forbidden permutations. We demonstrate that our simplified method, validated by chaotic and reversible model series and their surrogates, is equivalent to methods measuring the probabilistic difference between forward–backward vectors and the probabilistic difference between symmetric vectors. In characterizing epileptic brain electric activities, seizure electroencephalograms (EEGs) have the strongest qTIR due to the development of synchronous neuronal firing, and the qTIR of seizure-free EEGs lies between that of the healthy control and ictal EEGs. Overall, we conduct a comprehensive analysis of permutation-based qTIR for nonlinearity detection, and our findings regarding qTIR in epileptic EEGs improve our understanding of nonequilibrium epileptic brain electrical activity and might even contribute to predicting epileptic seizures.

Keywords Time irreversibility · Permutation · Epilepsy · Seizure-free interval · EEG

W. Yao · D. Yao · D. Guo (✉)
The Clinical Hospital of Chengdu Brain Science Institute, MOE Key Lab for NeuroInformation, Center for Information in Medicine, School of Life Science and Technology, University of Electronic Science and Technology of China, Chengdu 611731, China
e-mail: dqguo@uestc.edu.cn

W. Yao · J. Wang
Smart Health Big Data Analysis and Location Services Engineering Lab of Jiangsu Province, Nanjing University of Posts and Telecommunications, Nanjing 210023, Jiangsu, China

J. Dai
Department of Neurology, Jinling Hospital, Medical School of Nanjing University, Nanjing 210002, Jiangsu, China

M. Perc
Faculty of Natural Sciences and Mathematics, University of Maribor, Koroška cesta 160, 2000 Maribor, Slovenia

M. Perc
Complexity Science Hub Vienna, Josefstädterstraße 39, 1080 Vienna, Austria

1 Introduction

The brain, a collection of vast numbers of neurons and glial cells, is a typical complex system [1] and is affected by various physiological and pathological conditions, e.g., life-threatening epilepsy. As one of the most common severe neurological diseases characterized by recurrent seizures, epilepsy can also cause social isolation, stigmatization and disability, and the stigma of epilepsy has additional negative effects on

the families of individuals with the disorder [2]. Important theoretical and experimental advances [3], including nonlinear methods, have been applied to characterize brain electrical and magnetic activities to understand and elucidate the pathophysiological mechanisms underlying the neurological condition. Among nonlinear approaches [4], low-dimensional nonlinearities have long been evaluated for the feature extraction of epileptic signals [5–9], and causality coupling (e.g., transfer entropy [10] and phase synchronization [11]) has also been used to reveal epileptic brain connections [12]. Network science currently presents a welcome opportunity to facilitate the networked models and features of the epileptic process [13–15]. Due to the inherent complexity of the brain [4,16], nonlinear measures have been gaining popularity for exploring the dynamic behaviors of epileptic brain activity.

Another fundamental property of nonequilibrium complex processes is time irreversibility (TIR), which has attracted substantial attention in recent research for characterizing complex dynamical systems. The TIR and temporal asymmetry (TAS) of heartbeats have been widely proved to be linked to cardiac autonomic regulation [17,18], and broken asymmetry in aging and diseased heart rates has been demonstrated in several reports [19–21]. TIR has also been used to reveal the nonequilibrium behavioral variability in active living microorganisms [22]. In addition to physiological and biological areas, TIR is advantageous for nonlinear detection in other complex signals, such as economic data [23,24], turbulent flows [25] and physical phenomena [26]. However, as a manifestation of complex brain signals, TIR has not been widely applied to explore the nonequilibrium characteristics of epileptic brain activities for reasons including the challenges of quantitative time irreversibility (qTIR).

Time reversibility describes the invariant statistical properties of processes under a reversal timescale [27,28]; however, qTIR is involved in measuring the probabilistic differences between symmetric or between forward-backward joint distributions, which is not trivial. The traditional linear entropy estimators or kernel methods are not designed for the symmetric or forward–backward vectors of qTIR; therefore, several alternative approaches that simplify the time series of nonequilibrium processes have been proposed for qTIR. Guzik [17], Porta et al. [18,29] and Costa et al. [19,20] transformed time series into ups and downs. Lacasa et al. [23,30] mapped the process onto a horizontal visibility graph and measured the in–out difference for qTIR. Yao et al. [21], Zanin et al. [31], Martínez et al. [32] and Li et al. [33] applied permutations as alternatives to raw vectors. Symbolic approaches [34–37] that transform time series into symbolic sequences have also been employed for their simplicity, robustness, speed, insensitivity to noise, etc. In these approaches, some detailed information is lost or some symbolic templates are lacking, but the effects of these issues on qTIR have not received adequate attention. Moreover, the concepts of TIR and TAS are arguably equivalent in characterizing nonequilibrium processes; however, the implicit associations between them have not been investigated.

To address these issues, we use equal-value permutations to simplify qTIR and detect nonequilibrium features in epileptic electroencephalograms (EEGs). Our research verifies the effects of the simplified time series on qTIR and bridges the TIR and TAS theoretically and experimentally by connecting the forward–backward process and symmetric vectors. The application of qTIR in epileptic EEGs improves our understanding of the nonequilibrium characteristics and particularly the abnormally high TIR of epileptic brain electrical signals.

2 Quantitative time irreversibility

2.1 Basic definitions of time reversibility

Time reversibility describes the invariant probabilistic properties of a process with respect to time reversal. Here, we present two statistical definitions for time reversibility.

Definition 1 In the definition of Weiss [27], a stationary process $X(t)$ is time reversible if $\{X(t_1), X(t_2), \ldots, X(t_m)\}$ and $\{X(-t_1), (-t_2), \ldots, X(-t_m)\}$ have the same joint probability distributions for every $t_1, t_2, \ldots, t_m$ and m.

Definition 2 An alternative definition due to Kelly [38] suggests that if $X(t)$ is reversible, $\{X(t_1), X(t_2), \ldots, X(t_m)\}$ and $\{X(-t_1 + n), X(-t_2 + n), \ldots, X(-t_m+n)\}$ have the same joint probability distribution for every n and m, under which $\{X(t_1), X(t_2), \ldots, X(t_m)\}$ have the same probability distribution with its symmetric vector $\{X(t_m), \ldots, X(t_2), X(t_1)\}$ if $n = t_1 + t_m$.

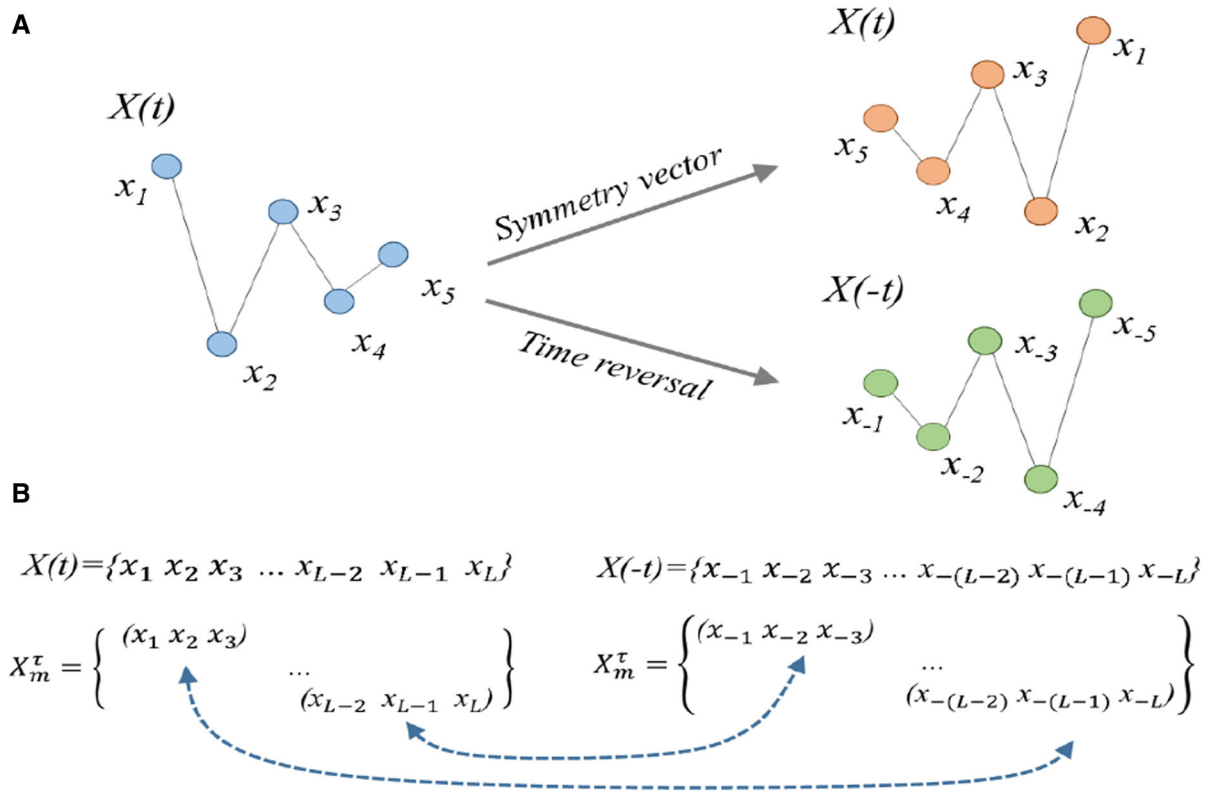

Fig. 1 Exemplary illustration of the vector and its symmetric form and the corresponding vector in reverse time series. **a** For $(x_1, x_2, x_3, x_4, x_5)$ in time series $X(t)$, the symmetric vector $(x_5, x_4, x_3, x_2, x_1)$ is the same as the corresponding vector $(x_{-1}, x_{-2}, x_{-3}, x_{-4}, x_{-5})$ in time reversal $X(-t)$. **b** Corresponding multidimensional vectors in $X(t)$ and $X(-t)$

We should note that although Definition 2 does not impose the condition of stationarity, it shows that time reversibility implies stationarity. The two definitions of time reversibility both require the time reversible process to be stationary, suggesting that time reversible processes are a subset of stationary ones [38], i.e., time reversibility implies stationary, but not vice versa.

Time irreversibility can be quantified from two perspectives, namely the probabilistic difference between the forward and its backward processes, i.e., TIR, and the probabilistic differences between the symmetric joint distributions of a process, i.e., TAS. From the visual perspective illustrated in Fig. 1, for the vector $(x_1, x_2, \ldots, x_t)$ in time series $X(t)$, its symmetric vector $(x_t, \ldots, x_2, x_1)$ and corresponding vector $(x_{-1}, x_{-2}, \ldots, x_{-t})$ in the reversible time series $X(-t)$ are in fact the same.

2.2 Simplified alternative: order patterns

Due to the difficult calculation of the probabilistic differences in joint distributions, simplified quantifications of TIR are widely adopted in the relevant literature [17–23,29–37]. Among these simplifications, a method based on permutation, originally introduced by Bandt and Pompe for the permutation entropy (PEn) [39], comes naturally from the time series and shares mathematical similarity with the multidimensional vector, which is particularly relevant in qTIR.

Let us briefly introduce the permutation method. We first construct m-dimensional vectors as follows:

$$X_m^\tau = \{x(t), x(t+\tau), \ldots, x(t+(m-1)\tau)\} \quad (1)$$

for dimension m and time delay τ. Then, we organize the elements according to their relative values, e.g., in ascending order $x(j_1) < x(j_2) < \cdots < x(j_i)$ or in descending order $x(j_1) > x(j_2) > \cdots > x(j_i)$, and obtain the order pattern, $\pi_i = \{j_1, j_2, \ldots, j_i\}$, i.e., the

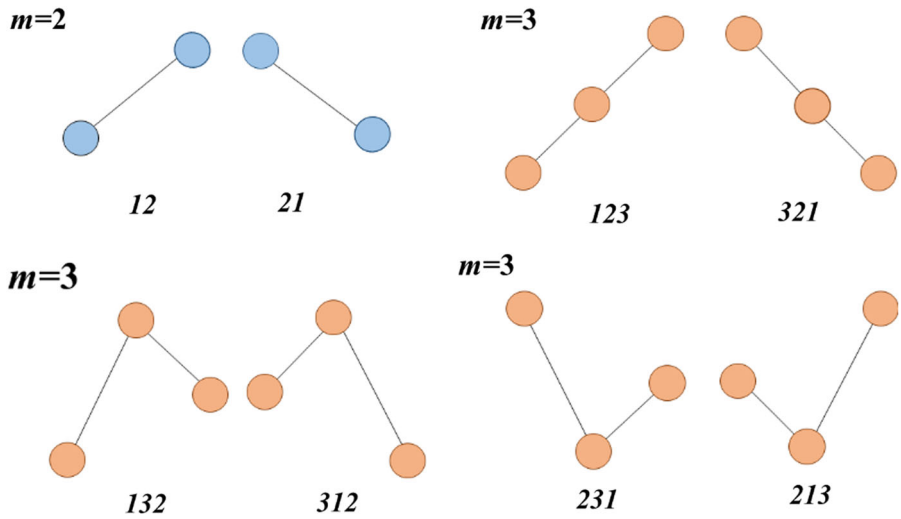

Fig. 2 Order patterns when m is 2 and 3. Taking equal values out of consideration, the upper bound of the amount of permutation is m!, e.g., the 2 (2!) symmetric order patterns, namely up ('12') and down ('21') in top left two figures, when $m = 2$, and the 6 (3!) permutations when $m = 3$. Vectors are illustrated as 4 pairs of symmetric forms

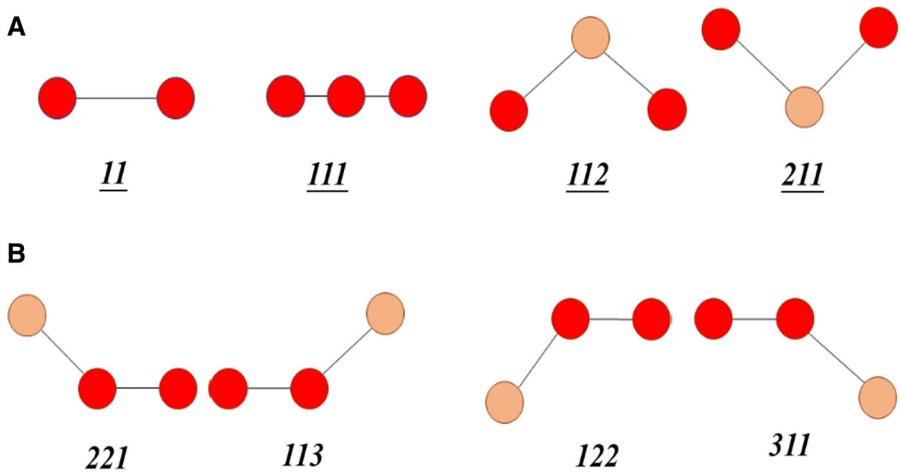

Fig. 3 Equal-value order patterns when m is 2 and 3. **a** Four underlined permutations of self-symmetric vectors, including 2 all-equal vectors ('11' and '111') and 2 three-value vectors whose permutations are '112' and '211.' **b** Two pairs of symmetric vectors with double-equal values when $m = 3$. Equal values in each vector are in red color. (Color figure online)

vector of indexes. Figure 2 illustrates the 2 and 6 order patterns when $m = 2$ and 3, respectively.

In permutation-based TIR analysis, equal values not only change the generation and distributions of order types but also lead to self-symmetric permutation (i.e., the permutation whose symmetric pattern is itself) [21,40]; therefore, we employ the equal-value ordinal scheme proposed by Bian et al. [41] for reliable qTIR. To construct equal-value permutations, we must organize the equal values in adjacent continuous orders according to the order of their occurrence, e.g., the double-equal $x\,(j_m) = x(j_n)$ and triple-equal $x\,(j_x) = x\,(j_y) = x\,(j_z)$, and then modify the indexes of equal values to the smallest ones in each individual group of adjacent continuous orders, i.e., the $\{j_m, j_m\}$ and $\{j_x, j_x, j_x\}$. In the equal-value ordinal scheme, there are more order patterns, and more importantly, there are self-symmetric forms, e.g., the all-equal permutations '1111...' and other symmetric ones such as '112' and '211,' as shown in Fig. 3.

2.3 Subtraction-based parameters for probabilistic difference

Given the existence of forbidden permutations, there might be order patterns that do not simultaneously exist in the forward and backward series or do not have corresponding symmetric vector forms [21,42]. Division-based parameters, e.g., the Kullback–Leibler or Chernoff distance, for the probabilistic difference between existing and forbidden permutations are zero or infinity, unsuitable for the quantification of time irreversibility.

For the subtraction-based parameters for qTIR, there are Y_s [21,42], the Chi-square statistics χ^2 [34–36] and the Euclidean norm, illustrated in Eqs. 2, 3 and 4. Of the Y_s, $p(\pi_i)$ should not be smaller than $p(\pi_s)$.

$$Y_s\langle p(\pi_i), p(\pi_s)\rangle = \sum\nolimits_i p(\pi_i)\frac{p(\pi_i)-p(\pi_s)}{p(\pi_i)+p(\pi_s)} \tag{2}$$

$$\chi^2\langle p(\pi_i), p(\pi_s)\rangle = \sum\nolimits_i \frac{[p(\pi_i)-p(\pi_s)]^2}{p(\pi_i)+p(\pi_s)} \tag{3}$$

$$T\langle p(\pi_i), p(\pi_s)\rangle = \sqrt{\sum(p(\pi_i)-p(\pi_s)^2} \tag{4}$$

The subtraction-based parameters should have the following basic characteristics: (1) when $p(\pi_i)$ is equal to $p(\pi_s)$, their difference is 0; (2) if $p(\pi_s)$ is zero, the results should be accountable that the three parameters share the result of $p(\pi_i)$; (3) when the absolute differences between different pairs of $p(\pi_i)$ and $p(\pi_s)$ are the same, there is an additional parameter to adjust the difference as $k*[p(\pi_i)-p(\pi_s)]$, where k is $p(\pi_i)/[p(\pi_i)+p(\pi_s)]$ and $[p(\pi_i)-p(\pi_s)]/[p(\pi_i)+p(\pi_s)]$ in Y_s and χ^2, while the Euclidean distance T does not satisfy this condition. Therefore, to reliably measure the probabilistic difference of order patterns for qTIR, we employ Y_s and χ^2 in our paper.

To measure the rates of a single permutation that does not have its counterpart of the symmetric vector, we employ the parameter $R_u = N(\pi_\mu)/N(\pi)$ [42], where $N(\pi_\mu)$ is the number of single order patterns and $N(\pi)$ is the number of existing permutations.

qTIR could be simplified by measuring the probabilistic difference between the permutations of symmetric vectors (PSVs) or between the permutations of forward–backward vectors (PFBs).

3 Simplified qTIR in model processes

In this section, we generate irreversible chaotic and reversible Gaussian model series and construct their surrogate data by the improved amplitude adjusted Fourier transform (iAAFT) [43,44] to test the permutation-based qTIR. Of the chaotic models, the logistic equation [45], mathematically written as $x_{t+1} = r \cdot x_t(1 - x_t)$, is simple and deterministic, but can exhibit chaotic behavior. The Henon map [46], given by the coupled equations, $x_{t+1} = y_t + 1 - \alpha x_t^2$ and $y_{t+1} = \beta x_t$, presents a two-dimensional invertible iterated map with quadratic nonlinearity. The Lorenz system [47], generated by the three coupled differential equations, $\mathrm{d}x/\mathrm{d}t = \sigma(y-x)$, $\mathrm{d}y/\mathrm{d}t = x(r-z)\,y$ and $\mathrm{d}z/\mathrm{d}t = xy - bz$, is a simplified model originally constructed to represent forced dissipative hydrodynamic flow. The Y_s and χ^2 of the probabilistic differences among PSVs, PFBs and R_u of the three chaotic model series and Gaussian process are shown in Fig. 4.

As shown in Fig. 4, the Y_s and χ^2 of the three chaotic model series are all larger than the 97.5th percentile of the surrogate data. Of the reversible Gaussian process, the Y_s and χ^2 are between the 2.5th and 97.5th percentiles of its surrogate data sets. According to surrogate theory [44,48], the null hypothesis that the logistic, Henon and Lorenz series are linear is rejected, while the hypothesis that the Gaussian process is linear should be accepted, validating the effectiveness of Y_s and χ^2 for the quantification of time irreversibility.

In Sect. 2.1, we prove and illustrate that TIR and TAS are equivalent for the measurement of nonequilibrium, which is further verified by measurement of the same qTIR by Y_s and χ^2 of the probabilistic difference in the upper and lower 4 subplots, i.e., between the PSVs and between the PFBs, in Fig. 4. Conceptually speaking, we need to obtain the whole series and reverse it to calculate the TIR, which is not reliable for some real-time situations; therefore, the probabilistic difference between symmetric vectors (i.e., the TAS) is preferable for qTIR due to its computational simplicity and real-time characteristics.

The rate of single permutations has a close relationship with the time irreversibility of the four model series. R_u exhibits consistent changes with the Y_s and χ^2 for the chaotic processes particular for the logistic series. For the logistic series, when m is 5 or greater, the R_u, Y_s and χ^2 of the logistic series are all 1, i.e., there are no coexisting permutations for symmetric vectors and forward–backward vectors, and the R_u values for the linear Gaussian series are almost all zero. The close association between the R_u and qTIR suggests R_u may contain nonlinear structural features of dynamical complex systems, which will be discussed in the following section.

The chaotic and Gaussian processes have different nonlinearities due to their structural and dynamical differences, but they share the conclusion that it is equivalent to quantifying TIR and TAS by measuring the probabilistic differences between PSVs and between PFBs.

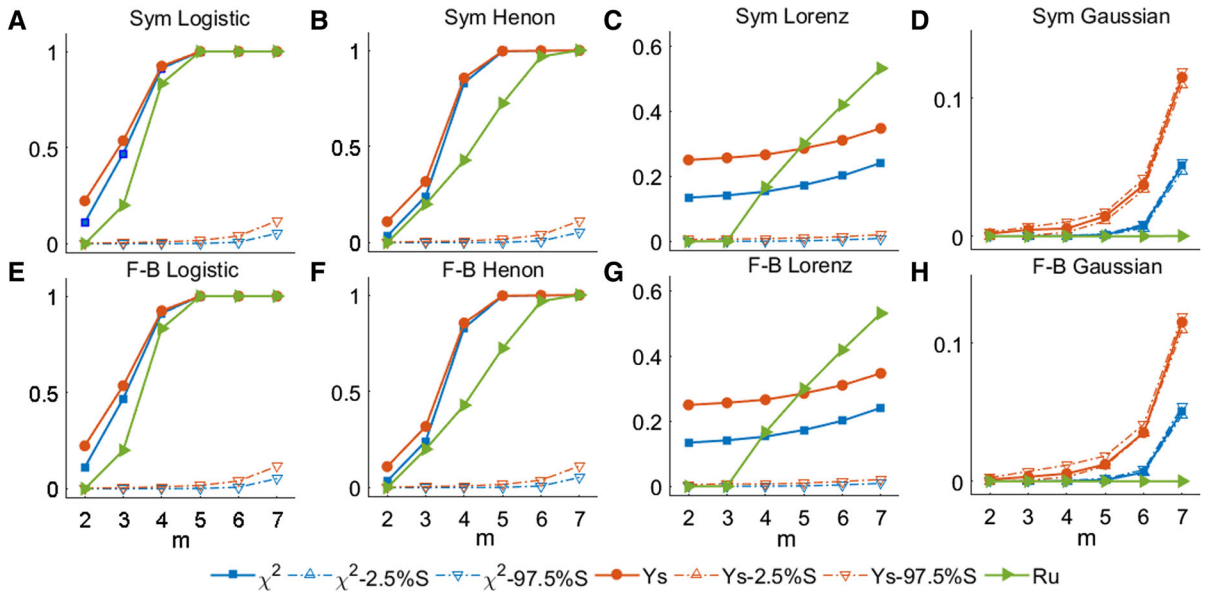

Fig. 4 Y_s and χ^2 of the chaotic series, reversible process and surrogate data. **a**, **b**, **c** and **d** Probabilistic differences between permutations of symmetric vectors titled with, e.g., the 'Sym logistic,' and **e**, **f**, **g** and **h** Probabilistic differences of permutations in forward and backward sequences titled with, e.g., the 'F–B logistic.' The 97.5th and 2.5th percentiles of the Y_s and χ^2 of the surrogate data are denoted 'Y_s-97.5%S,' 'Y_s-2.5%S,' 'χ^2-97.5%S' and 'χ^2-2.5%S.' The x-components of the logistic ($r = 4$, $x_1 = 0.01$), Henon ($\alpha = 1.4$, $\beta = 0.3$, and $x_1 = 0.01$, $y_1 = 0.01$) and Lorenz ($x_1 = 0$, $y_1 = 0$ and $z_1 = 1 \times 10^{-10}$, $\sigma = 10$, b $= 8/3$ and $r = 28$) equations are used to generate nonlinear series, and linear reversible Gaussian white noise is constructed. We set the upper bound of m to 7 and the data length to $10*(7!)=50400$ to achieve reliable nonlinearity detection

4 qTIR in epileptic brain electrical activities

The brain is a typical complex system with nonequilibrium features that are affected by the pathological condition of epilepsy. In this section, we detect the qTIR of brain electric data and analyze the effects of epilepsy on nonlinear EEGs.

4.1 Epileptic EEGs and the rate of single permutation

We selected two groups of EEGs, namely public Bonn epileptic data and induced epileptic recordings from Sprague–Dawley (SD) rats, to analyze qTIR under different conditions.

Of the Bonn data, there are 5 sets (denoted A–E) of EEG data, of which sets A (eyes open) and B (eyes closed) were recorded from healthy volunteers by surface electrodes. Sets D and C (both seizure-free) were collected, respectively, from within the epileptogenic zone and from the hippocampal formation of the opposite hemisphere was obtained through intracranial electrodes, and set E was taken from all the intracranial electrodes and only contained seizure activity [8]. Each data set contains 100 single-channel EEG recordings with a 173.61 sampling rate over a duration of 23.6 s.

For comparison, we applied the animal epilepsy pilocarpine model to 8 male SD rats in accordance with the Animal Care Guide for the Care and Use of Experimental Animals at the University of Electronic Science and Technology of China. Briefly, these pilocarpine-induced epileptic data were from our previous experimental study, and detailed information can be found in [49]. We selected 4 stages, namely the baseline (BL) stage, the pre-ictal (PreI) stage, the ictal stage and the post-ictal (PosI) stage, for our analysis. The BL stage refers to the period before drug injection, and the PreI stage is between the pilocarpine injection and the onset of status epilepticus (SE) discharge. The ictal stage is the period with continuous SE discharges following the PreI stage, and the PosI stage is approximately two hours after the onset of SE discharge and before the diazepam injection. Pilocarpine and diazepam injections were used to induce and stop seizures, respec-

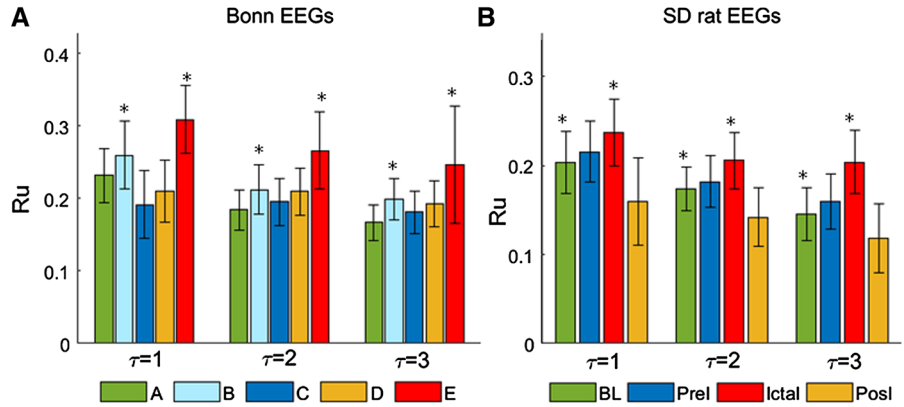

Fig. 5 R_u (mean ±std) of the Bonn in **a** and SD rat epileptic EEGs in **b**. R_u of $m = 2$ and 3 are all zeros that all of the existent permutations of vectors in Figs. 2 and 3 have their corresponding forms, and R_u of $m = 4$ for some sets of Bonn and SD rat EEGs are also zeros. The highest R_u values of EEGs during seizures, set E from the Bonn data and Ictal data from SD rats, are marked in red. *Represents the R_u of the set of EEGs is significantly different ($p < 0.0001$) from that of each other data set. Independent sample t test for Bonn EEGs and paired sample t test for SD rat EEGs is employed. (Color figure online)

tively. All rats had 10 implanted electrodes, consisting of 5 cortical electrodes, 4 depth electrodes and a reference electrode. Of all 8 rats under the 4 stages, we selected 4 segments with a duration of 9 s (9000 samples). Recordings with a sampling frequency of 1000 Hz were filtered by a band-pass filter of 0.16 Hz and 100 Hz.

Due to the difference between sets of Bonn EEGs in methods (i.e., from scalp or intracranial electrodes) and positions (i.e., within the epileptogenic zone and from the hippocampal formation of the opposite hemisphere), we employed the independent sample t test. And because the methods and positions of the SD rat EEGs under 4 stages are the same, we employed paired sample t test for the quantifiers of EEGs under each two different conditions.

R_u of the Bonn and SD rat EEGs are shown in Fig. 5. Considering the requirement for data length, we set the upper bound of m to 5 for the two sets of EEGs.

For the Bonn EEG, the R_u values of the healthy EEGs (sets A and B) were lower than those of the seizure EEG (set E), but larger than those of the seizure-free data (sets C and D). As in the Bonn EEGs, the seizure ictal data of the SD rats had the highest rates of single permutation, and the PreI data had higher R_u values than the BL data, while the PosI data had the lowest R_u. These observations suggest that there are extensive forbidden permutations in real-world physiological activity, resulting in some order patterns of vectors without corresponding forms. Moreover, the rates of single permutation are associated with features of the Bonn and SD EEGs: The R_u of the seizure EEGs was the highest, in line with the abnormal high nonlinear and firing brain activities.

The rate of single permutations derived from forbidden order patterns is associated with the features of complex systems, which might contribute to the nonlinear analysis of dynamical processes. Moreover, forbidden permutations in real-world EEGs further prove that division-based parameters are unsuitable for measuring probabilistic differences.

4.2 qTIR of the two groups of epileptic EEGs

We now explore the detection of the qTIR in the Bonn and SD rat epileptic EEGs. The Y_s and χ^2 of the probabilistic difference between PSVs of the Bonn and SD rat EEGs are shown in Figs. 6 and 7.

The seizure brain electric activities, set E from the Bonn data and ictal stage from the SD rat data, have the highest qTIR, as shown in Figs. 6 and 7. The discrimination between Bonn seizure EEG data and healthy data, namely A–E (Y_s, $p < 5.0\text{E}{-16}$; χ^2, $p < 10\text{E}{-8}$) and B–E (Y_s, $p < 1.0\text{E}{-14}$; χ^2, $p < 5.0\text{E}{-8}$), and that between seizure and seizure-free EEG data, namely C–E (Y_s, $p < 5.0\text{E}{-15}$; χ^2, $p < 1.0\text{E}{-8}$) and D–E (Y_s, $p < 1.0\text{E}{-11}$; χ^2, $p < 5.0\text{E}{-7}$), are statistically significant. For the SD rat EEGs, the ictal brain data also

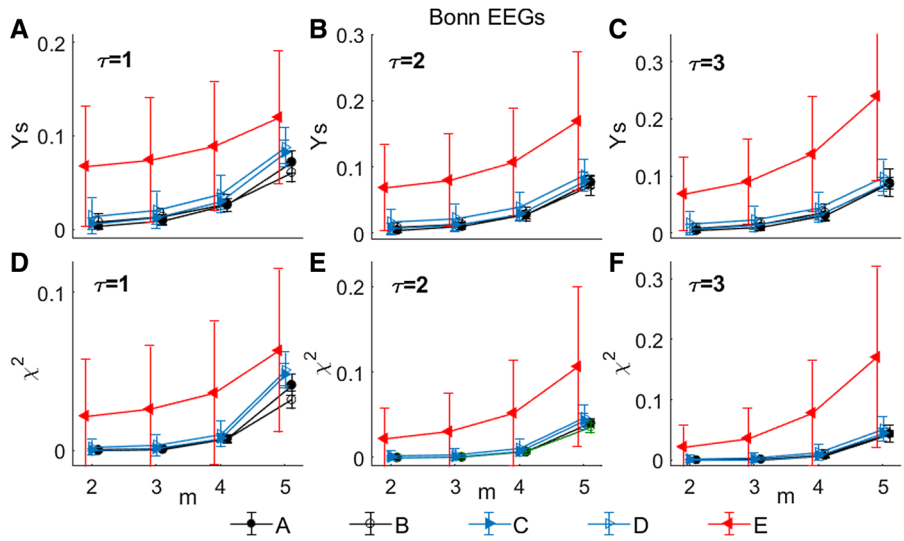

Fig. 6 Y_s and χ^2 (mean $\pm$ std) of the Bonn epileptic EEG data. **a**, **b** and **c** Y_s for the qTIR of the Bonn epileptic data when $\tau = 1$–3 and $m = 2$–5. **d**, **e** and **f** χ^2 for the qTIR of the Bonn epileptic data when $\tau = 1$–3 and $m = 2$–5. The highest qTIR values of the seizure EEGs are in red. (Color figure online)

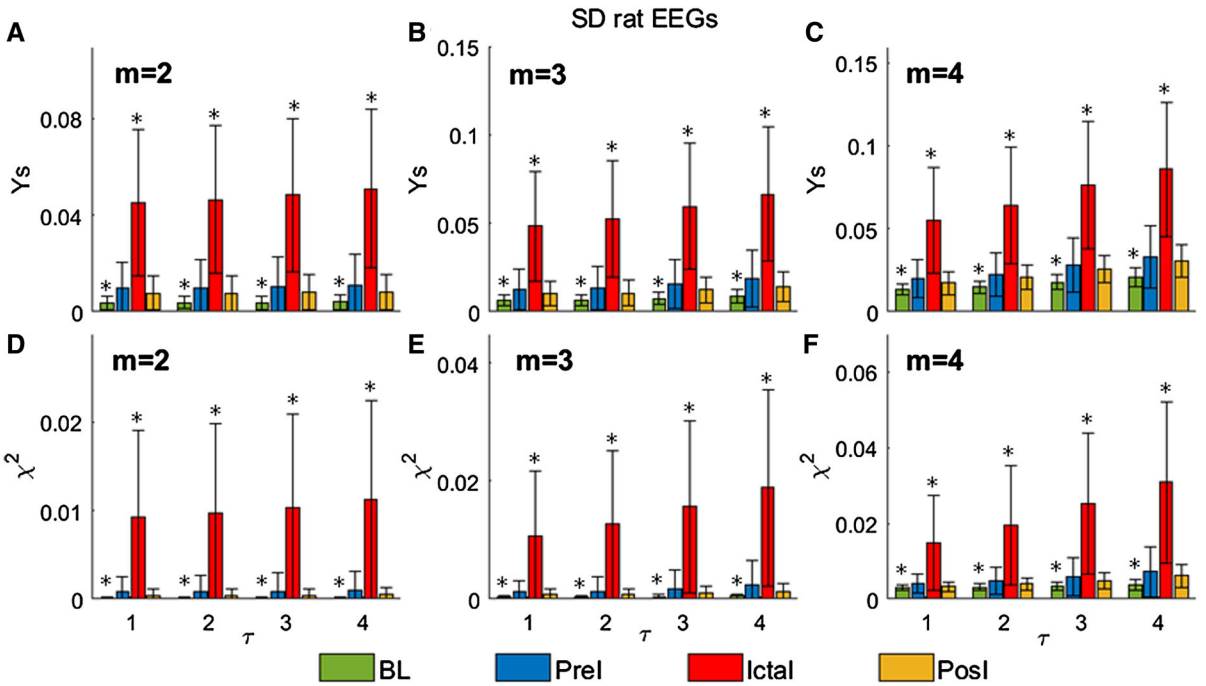

Fig. 7 Y_s and χ^2 (mean$\pm$std) of the SD rat epileptic EEG. **a**, **b** and **c** Y_s for the qTIR of the SD epileptic data when $\tau = 1$–5 and $m = 2$–4. **d**, **e** and **f** χ^2 for the qTIR of the Bonn epileptic data when $\tau = 1$–5 and **m** $= 2$–4. The highest qTIR values of the ictal seizure EEGs are in red. *Represents qTIR of the set of EEGs is significantly different ($p < 0.0001$) from that of each other data set. (Color figure online)

exhibited a significantly higher qTIR than the other 3 groups of EEGs, i.e., the BL-ictal (Y_s, $p <$ 1.0E–53; χ^2, $p <$ 1.0E–27), PreI-ictal (Y_s, $p <$ 1.0E-38; χ^2, $p <$ 1.0E–21) and PosI-ictal (Y_s, $p <$ 1.0E–45; χ^2, $p <$ 1.0E–25) discriminations were all statistically acceptable. The qTIR in the two groups of EEGs suggests that Y_s is preferable to χ^2 for the measurement of the probability difference. The pathological features

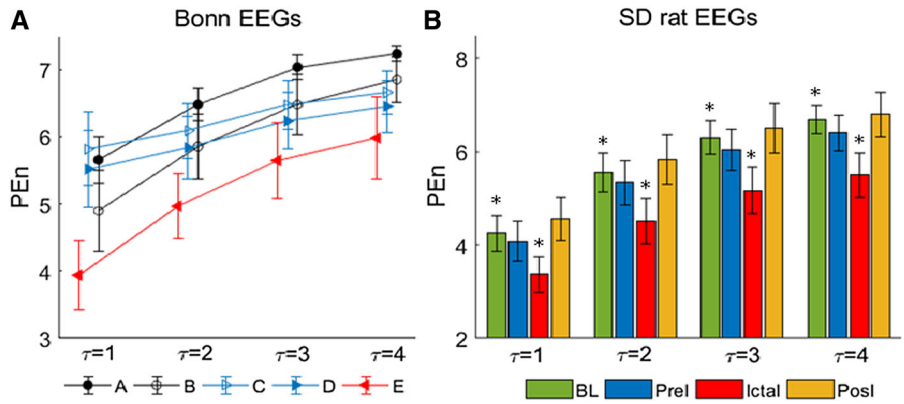

Fig. 8 PEn (mean± std) of $m = 5$ and $t = 1$–4 of the Bonn and SD rat epileptic EEGs. **a** Line chart of the PEn of the Bonn EEGs and **b** bar graph of the PEn of the SD rat EEGs. The lowest PEn values of seizure EEGs of both the Bonn and SD rat data sets are in red color. *Indicates a significant difference ($p < 0.0001$) between PEn of the EEGs and those of others

of epilepsy should account for the highest nonlinearity of the seizure EEG data. Epileptic seizures develop abruptly and last a few seconds, and the clinical onset of synchronous neuronal firing in the cerebral cortex can be recorded by intracranial or surface EEGs [16,49]. During seizures, the hallmark of epilepsy (i.e., recurrent seizures) leads to severely abnormal brain activities and dynamical disorders recorded by invasive or noninvasive EEGs with abnormally high nonlinearity. Our findings verify the significantly higher nonlinearity of brain activity in patients during seizures than in healthy control subjects and seizure-free patients.

Moreover, the Bonn and SD rat brain data also share the characteristic that the seizure-free EEGs had clearly higher qTIR than the control EEGs. Of the Bonn epileptic data, the Y_s-qTIR of the A–C ($p < 0.009$), A–D ($p < 0.0001$), B–C ($p < 0.05$) and B–D ($p < 0.005$) differences were acceptable, and of the SD rat EEGs, the Y_s-qTIR of the BL-PreI ($p < 5.0\text{E}{-10}$) and BL-PosI ($p < 1.0\text{E}{-11}$) comparisons were also significantly different. In the original publication of the Bonn EEGs [8], the nonlinear prediction error and correlation dimension of the seizure-free sets were reported to be between the values of the healthy (the lowest) and the seizure (the strongest) sets, which was confirmed by other papers involving the Bonn data sets [50,51]. After seizure onset, partial seizures may also remain localized and cause abnormal brain nonlinear activities [16], and before the onset of SE discharges, the human and rat brains might have some induced abnormal electric activity that increases the nonequilibrium features. Our findings, particularly those in the SD rat EEGs about the higher qTIR in the PreI stage, might contribute to epilepsy prediction.

To compare with qTIR, we employ the closely related statistical parameter, Shannon entropy, i.e., the permutation entropy (PEn), also based on equal-value ordinal scheme, in an analysis of the two groups of EEGs, and show the results in Fig. 8.

Figure 8 demonstrates that the PEn values of the EEGs are generally contradictory to the qTIR, sharing the conclusions in the previous report provided by the present authors. Basically, the higher the qTIR of EEGs, the lower the PEn, e.g., the epileptic EEGs of the Bonn E data set and SD rat ictal data set have the smallest PEn, but the largest qTIR among those of the other data sets. The PEn of the Bonn data in Fig. 8a is not stable, with the relative relationships changing with the time delay, in contrast to the stable results of qTIR. For the SD rat EEGs in Fig. 8b, we found that the discrimination between the PEn of BL as well as of Ictal EEGs and PEn of others, although statistically acceptable ($p < 0.0001$), are not significant than those between the Ys-based qTIR of the EEGs. Therefore, PEn does not have an advantage in stability or feature extraction compared to qTIR in these two groups of epileptic EEGs.

Overall, qTIR, particularly that based on the Y_s, is a reliable statistical parameter for characterizing complex brain electric activity.

5 Discussion

According to our analysis, two issues regarding permutation-based qTIR and one regarding its application in epileptic EEGs need further discussion.

In the symbolic ordinal scheme, forbidden permutations play an important role in nonlinear dynamics

analysis, especially time irreversibility. Forbidden permutations not only impact the simplified qTIR but also contain important structural or dynamic information about dynamical processes [52]. Of the three chaotic series, qTIR shows similar changes in the rate of single permutations. The R_u values of the Gaussian process are all 0, which are associated with reversibility. Analysis of the Bonn and SD rat EEGs revealed that the highest rates of single permutations were consistent with the highest qTIR. The characteristics of forbidden order patterns have been studied in depth due to their close connections to dynamical complexity and structural information [42,52–56]. The single permutation rate quantifies the forbidden permutations and suggests a reliable connection with the properties of the model and real-world time series. However, the seizure-free EEGs in the Bonn data sets (particularly set C) and those from SD rats (in the PosI stage) exhibited lower rates of single order patterns than those in the control sets; therefore, R_u as a nonlinear parameter needs further investigation, although it contributes to the exploration of dynamical complex systems.

Another issue regarding qTIR is the relationship between symmetric permutations (SPs) and PSVs. PSVs are preferable for qTIR in real-time situations because they do not require the whole series needed by the forward–backward methods; however, in some simplified qTIR models, the misuse of SPs and PSVs might yield some conceptual mistakes. Some scholars [31,42] use SPs or symmetric symbolizations to simplify the quantification of time irreversibility. In fact, SPs are not equivalent to the PSV (more relevant to the time irreversibility) unless the vectors are center-based symmetric. These simplifications effectively characterize the nonlinearity of complex systems; however, they are not directly relevant to time irreversibility. Moreover, the probability difference between SPs and between PSVs and even the probabilistic difference of all permutations (PDP) [57] are all effective in characterizing the nonlinearity of time series, and when $m = 2$, they are all the same. Therefore, the probabilistic difference of permutations or symbolic templates for simplifying nonlinearity detection and characterizing the structural or dynamical features of complex systems deserves more comprehensive investigation.

The findings for the comparative analysis of Shannon entropy and qTIR revealed similar conclusions to those in our previous paper [40] with some exceptions. Shannon entropy calculates the amount of information for each individual probability, while qTIR targets the difference between paired probabilities. The two statistical parameters are generally different and even contradictory in their characterization of complex systems, e.g., the heartbeats from public PhysioNet [40]; however, under some extreme conditions, the two indexes might have consistent changes, e.g., the epileptic data in our study. PosI EEGs were shown to have both PEn and qTIR higher than BL EEGs from SD rats, suggesting that PosI brain electric activities have both nonlinear complexity and nonequilibrium higher than BL activities. Moreover, in our previous analysis of the epileptic EEGs from Jinling Hospital, we found that the healthy control EEGs also had both larger time irreversibility [42] and Shannon entropy [58]. Therefore, the relationship between Shannon entropy and qTIR is more complex than simply contradictory or consistent and requires more related comprehensive comparative analysis of the two statistical quantifiers with larger and more representative data sets.

The manifestation of high nonlinearity in seizure EEGs has been demonstrated by most reports; however, some sets of EEGs, e.g., from the Bonn sets A and B, in our analysis are compatible with the Gaussian linear stochastic series, sharing the findings in the original introduction of Bonn data [8]. Andrzejak et al. amused that the acceptance of null hypothesis for the Bonn sets of A might originate from the large numbers of neurons and the complex structure of brain, and they proposed that the reasons might reside in that the dynamical structures in surface EEGs might be blurred by filter processes by due to different conductivities of the skull and other tissues [8]. The brain is arguably a complex collection of hundreds of billions of neurons and more glial cells that interact and synchronize with each other, and brain behaviors are subject to internal physiological factors and external environmental influence. However, it is just the typical complex brain system that the brain electronic activities should be typical nonlinear processes [42], and certain constraints imposed on EEGs might be the rooted reasons that demask nonlinear deterministic traits of neuronal dynamics [8]. Moreover, regarding the properties of epileptic and healthy brain dynamics, spike-timing-dependent plasticity (STDP), by which neurons modify synaptic strength to adapt neuronal activity, adds a relevant amount of complexity to the dynamics of a neuronal network. The key role of plasticity and, in particular, the emergence of seizure-related nonlinear

dynamical features in the brain may also be attributed to the presence of propagation delays and their interplay with the synaptic weights in plastic neuronal networks [59,60]. In fact, STDP may determine the dynamics of the nonepileptic basin of attraction in multistable epileptic neuronal networks where perturbations can cause unstable situations resulting in epileptic seizures [61]. This notion can shed light on the physiological mechanisms behind seizure generation and propagation in the brain, where the regulation of emergent nonlinear dynamical features can be considered to shift the dynamics of the epileptic brain toward healthy attractor states.

Regarding seizure-free epileptic EEGs, there are some reports [42,58] suggesting that the brain electrical activity of seizure-free epileptic patients has lower nonlinearity than that of healthy subjects, which is inconsistent with our findings. From the physiological and pathological perspective, the manifestation of cyclic rhythm [62,63] in human epilepsy may affect the nonlinear detection of seizure-free EEGs. The time between seizure-free brain recordings and seizures plays an important role in the detection of nonlinear dynamical features in the brain. Soon after seizure onset, partial seizures may also remain localized and cause abnormal brain nonlinear activities [16]; however, after a long period (e.g., 20 or 30 days), the patients might have lower nonlinear brain activity than healthy individuals [42,58]. From high nonlinear activity during seizures to nonlinearity lower than that in healthy individuals, the nonlinear dynamics of the brain behaviors may also be related to circadian rhythms, and the brain activity during different epileptic stages, even in seizure-free intervals, could show totally different nonlinear features. Considering the circadian and circaseptan rhythms in human epilepsy, patients in different stages of epilepsy might have completely different brain behaviors, resulting in different nonlinear characteristics of two kinds of seizure-free EEGs, even when both are collected in seizure-free intervals. Accordingly, we hypothesize that the nonlinearity of brain activities in human epilepsy is also characterized by circadian rhythms. The rates of seizures oscillate in cycles of days, months and years, and seizure cycles are subject to various factors, including stress levels, sleep quality, other innate biological drivers and unknown reasons [62,63]. And due to the difference among epileptic patients and the difference in the periods for data collection particular the time from the ictal seizures, it is possible that EEGs under seizure-free intervals have different or even contradictory nonlinearity. Therefore, our hypothesis about circadian nonlinearity in epileptic EEGs needs to be verified by a large amount of data and more representative studies.

6 Conclusions

In summary, the nonlinearity of epileptic EEGs is characterized by permutation-based qTIR in this paper. We proved that the probabilistic divergence between symmetric vectors (i.e., TAS) is equivalent to that between the forward and back-ward processes (i.e., TIR). We verified the effects of forbidden permutations on the simplified qTIR and clarified the effectiveness of PSVs, as distinct from SPs, for simplified qTIR. The single permutation rate is in line with the qTIR in chaotic and Gaussian series and real-world EEGs, indicating its close association with the nonlinearity of the complex process. The abnormally high time irreversibility of the EEGs during seizures is in line with the fact that neuronal firing leads to abnormal dynamic brain activities. The higher qTIR in the pre-ictal stage provides valuable information for the prediction of epilepsy seizures.

Acknowledgements The project is supported by the National Natural Science Foundation of China (Grant Nos. 31671006, 61771251, 61527815, 31771149, 81571770, 61933003), the Sichuan Science and Technology Program (Grant No. 2018HH0003), the Jiangsu Provincial Key R&D Program (Social Development) (Grant Nos. BE2015700, BE2016773), the Natural Science Research Major Program in Universities of Jiangsu Province (Grant No. 16KJA310002), and the Slovenian Research Agency (Grant Nos. J4-9302, J1-9112 and P1-0403).

Compliance with ethical standards

Conflict of interest The authors declare that they have no conflict of interest.

Ethical approval All procedures performed in studies involving animals were in accordance with the ethical standards of the institution or practice at which the studies were conducted.

References

1. Suzana, H.H.: The human brain in numbers: a linearly scaled-up primate brain. Front. Human Neurosci. **3**, 31 (2009)
2. Banerjee, P.N., Filippi, D., Allen Hauser, W.: The descriptive epidemiology of epilepsy—a review. Epilepsy Res. **85**(1), 31–45 (2009)

3. Moshé, S.L., Perucca, E., Ryvlin, P., Tomson, T.: Epilepsy: new advances. Lancet **385**(9971), 884–898 (2015)
4. Stam, C.J.: Nonlinear dynamical analysis of EEG and MEG: review of an emerging field. Clin. Neurophysiol. **116**(10), 2266–2301 (2005)
5. Liu, X., Liu, H., Tang, Y., Gao, Q.: Fuzzy PID control of epileptiform spikes in a neural mass model. Nonlinear Dyn. **71**(1–2), 13–23 (2013)
6. Babloyantz, A., Destexhe, A.: Low-dimensional chaos in an instance of epilepsy. Proc. Natl. Acad. Sci. **83**(10), 3513–3517 (1986)
7. Lehnertz, K., Elger, C.E.: Can epileptic seizures be predicted? Evidence from nonlinear time series analysis of brain electrical activity. Phys. Rev. Lett. **80**(22), 5019 (1998)
8. Andrzejak, R.G., Lehnertz, K., Mormann, F., Rieke, C., David, P., Elger, C.E.: Indications of nonlinear deterministic and finite-dimensional structures in time series of brain electrical activity: dependence on recording region and brain state. Phys. Rev. E **64**(6 Pt 1), 061907 (2001)
9. Yao, W., Wang, J.: Multi-scale symbolic transfer entropy analysis of EEG. Phys. A Stat. Mech. Appl. **484**, 276–281 (2017)
10. Staniek, M., Lehnertz, K.: Symbolic transfer entropy. Phys. Rev. Lett. **100**(15), 158101 (2008)
11. Mormann, F., Lehnertz, K., David, P., Elger, C.E.: Mean phase coherence as a measure for phase synchronization and its application to the EEG of epilepsy patients. Phys. D Nonlinear Phenom. **144**(3–4), 358–369 (2000)
12. Fan, D., Zhang, L., Wang, Q.: Transition dynamics and adaptive synchronization of time-delay interconnected corticothalamic systems via nonlinear control. Nonlinear Dyn. **94**(4), 2807–2825 (2018)
13. Lehnertz, K., Ansmann, G., Bialonski, S., Dickten, H., Geier, C., Porz, S.: Evolving networks in the human epileptic brain. Phys. D Nonlinear Phenom. **267**(1), 7–15 (2014)
14. Ghosh-Dastidar, S., Adeli, H., Dadmehr, N.: Mixed-band wavelet-chaos-neural network methodology for epilepsy and epileptic seizure detection. IEEE Trans. Biomed. Eng. **54**(9), 1545–1551 (2007)
15. Bullmore, E., Sporns, O.: Complex brain networks: graph theoretical analysis of structural and functional systems. Nat. Rev. Neurosci. **10**(3), 186–198 (2009)
16. Iasemidis, L.D.: Epileptic seizure prediction and control. IEEE Trans. Biomed. Eng. **50**(5), 549–558 (2003)
17. Guzik, P., Piskorski, J., Krauze, T., Wykretowicz, A., Wysocki, H.: Heart rate asymmetry by Poincaré plots of RR intervals. Biomed Tech Biomed Eng **51**(4), 272–275 (2006)
18. Porta, A., Guzzetti, S., Montano, N., Gnecchi-Ruscone, T., Furlan, R., Malliani, A.: Time reversibility in short-term heart period variability. In: Computers in Cardiology, pp. 77–80. IEEE (2006)
19. Costa, M.D., Goldberger, A.L., Peng, C.K.: Broken asymmetry of the human heartbeat: loss of time irreversibility in aging and disease. Phys. Rev. Lett. **95**(19), 198102 (2005)
20. Costa, M.D., Peng, C.K., Goldberger, A.L.: Multiscale analysis of heart rate dynamics: entropy and time irreversibility measures. Cardiovasc. Eng. **8**(2), 88–93 (2008)
21. Yao, W., Yao, W., Wang, J.: Equal heartbeat intervals and their effects on the nonlinearity of permutation-based time irreversibility in heart rate. Phys. Lett. A **383**(15), 1764–1771 (2019)
22. Wan, K.Y., Goldstein, R.E.: Time irreversibility and criticality in the motility of a flagellate microorganism. Phys. Rev. Lett. **121**(5), 058103 (2018)
23. Flanagan, R., Lacasa, L.: Irreversibility of financial time series: a graph-theoretical approach. Phys. Lett. A **380**(20), 1689–1697 (2016)
24. Yang, P., Shang, P.: Relative asynchronous index: a new measure for time series irreversibility. Nonlinear Dyn. **93**, 1–13 (2018)
25. Jucha, J., Xu, H., Pumir, A., Bodenschatz, E.: Time-reversal-symmetry breaking in turbulence. Phys. Rev. Lett. **113**(5), 054501 (2014)
26. Brunelli, M., Fusco, L., Landig, R., Wieczorek, W., Hoelscher-Obermaier, J., Landi, G., Semião, F.L., Ferraro, A., Kiesel, N., Donner, T., De Chiara, G., Paternostro, M.: Experimental determination of irreversible entropy production in out-of-equilibrium mesoscopic quantum systems. Phys. Rev. Lett. **121**(16), 160604 (2018)
27. Weiss, G.: Time-reversibility of linear stochastic processes. J. Appl. Probab. **12**(4), 831–836 (1975)
28. Ramsey, J.B., Rothman, P.: Time irreversibility and business cycle asymmetry. J. Money Credit Bank. **28**(1), 1–21 (1995)
29. Porta, A., Casali, K.R., Casali, A.G., Gnecchi-Ruscone, T., Tobaldini, E., Montano, N., Lange, S., Geue, D., Cysarz, D., Van Leeuwen, P.: Temporal asymmetries of short-term heart period variability are linked to autonomic regulation. Am. J. Physiol. Regul. Integr. Comp. Physiol. **295**(2), 550–557 (2008)
30. Lacasa, L., Nunez, A., Roldan, E., Parrondo, J.M.R., Luque, B.: Time series irreversibility: a visibility graph approach. Eur. Phys. J. B **85**(6), 217 (2012)
31. Zanin, M., Rodríguez-González, A., Menasalvas Ruiz, E., Papo, D.: Assessing time series reversibility through permutation patterns. Entropy **20**(9), 665 (2018)
32. Martínez, J.H., Herrera-Diestra, J.L., Chavez, M.: Detection of time reversibility in time series by ordinal patterns analysis. Chaos Interdiscip. J. Nonlinear Sci. **28**(12), 123111 (2018)
33. Li, J., Shang, P., Zhang, X.: Time series irreversibility analysis using Jensen–Shannon divergence calculated by permutation pattern. Nonlinear Dyn. **96**(4), 2637–2652 (2019)
34. Daw, C.S., Finney, C.E.A., Kennel, M.B.: Symbolic approach for measuring temporal "irreversibility". Phys. Rev. E **62**(2), 1912 (2000)
35. Daw, C.S., Finney, C.E.A., Tracy, E.R.: A review of symbolic analysis of experimental data. Rev. Sci. Instrum. **74**(2), 915–930 (2003)
36. Kennel, M.B.: Testing time symmetry in time series using data compression dictionaries. Phys. Rev. E **69**(5), 056208 (2004)
37. Cammarota, C., Rogora, E.: Time reversal, symbolic series and irreversibility of human heartbeat. Chaos Solitons Fractals **32**(5), 1649–1654 (2007)
38. Kelly, F.P.: Reversibility and Stochastic Networks. Cambridge University Press, Cambridge (1979)
39. Bandt, C., Pompe, B.: Permutation entropy: a natural complexity measure for time series. Phys. Rev. Lett. **88**(17), 174102 (2002)
40. Yao, W., Yao, W., Yao, D., Guo, D., Wang, J.: Shannon entropy and quantitative time irreversibility for different and

even contradictory aspects of complex systems. Appl. Phys. Lett. **116**(1), 014101 (2020)
41. Bian, C., Qin, C., Ma, Q.D., Shen, Q.: Modified permutation-entropy analysis of heartbeat dynamics. Phys. Rev. E **85**(2 Pt 1), 021906 (2012)
42. Yao, W., Yao, W., Wang, J., Dai, J.: Quantifying time irreversibility using probabilistic differences between symmetric permutations. Phys. Lett. A **383**(8), 738–743 (2019)
43. Schreiber, T., Schmitz, A.: Improved surrogate data for nonlinearity tests. Phys. Rev. Lett. **77**(4), 635–638 (1996)
44. Schreiber, T., Schmitz, A.: Surrogate time series. Phys. D Nonlinear Phenom. **142**(3–4), 346–382 (2000)
45. May, R.M.: Simple mathematical models with very complicated dynamics. Nature **261**(5560), 459–467 (1976)
46. Henon, M.: A two-dimensional mapping with a strange attractor. Commun. Math. Phys. **50**(1), 69–77 (1976)
47. Lorenz, E.N.: Deterministic nonperiodic flow. J. Atmosph. Sci. **20**(2), 130–141 (1963)
48. Theiler, J., Eubank, S., Longtin, A., Galdrikian, B., Farmer, J.D.: Testing for nonlinearity in time series: the method of surrogate data. Phys. D Nonlinear Phenom. **58**(1–4), 77–94 (1992)
49. Cui, Y., Liu, J., Luo, Y., He, S., Xia, Y., Zhang, Y., Yao, D., Guo, D.: Aberrant connectivity during pilocarpine-induced status epilepticus. Int. J. Neural Syst. (2019). https://doi.org/10.1142/S0129065719500291
50. Donges, J.F., Donner, R.V., Kurths, J.: Testing time series irreversibility using complex network methods. Europhys. Lett. **102**(1), 381–392 (2013)
51. Kulp, C.W., Zunino, L., Osborne, T., Zawadzki, B.: Using missing ordinal patterns to detect nonlinearity in time series data. Phys. Rev. E **96**(2), 022218 (2017)
52. Amigo, J.M.: Permutation Complexity in Dynamical Systems: Ordinal Patterns, Permutation Entropy and All That. Springer, Berlin (2010)
53. D'Alessandro, G., Politi, A.: Hierarchical approach to complexity with applications to dynamical systems. Phys. Rev. Lett. **64**(14), 1609–1612 (1990)
54. Amigo, J.M., Kocarev, L., Szczepanski, J.: Order patterns and chaos. Phys. Lett. A **355**(1), 27–31 (2006)
55. Amigo, J.M., Zambrano, S., Sanjuán, M.A.: True and false forbidden patterns in deterministic and random dynamics. Europhys. Lett. **79**(5), 50001 (2007)
56. Carpi, L.C., Saco, P.M., Rosso, O.: Missing ordinal patterns in correlated noises. Phys. A Stat. Mech. Appl. **389**(10), 2020–2029 (2010)
57. Yao, W., Hou, F., Li, J., Wang, J.: Probabilistic divergence of permutations for nonlinearity detection. Phys. A Stat. Mech. Appl. **532**, 121802 (2019)
58. Yao, W., Liu, T., Dai, J., Wang, J.: Multiscale permutation entropy analysis of electroencephalogram. Acta Phys. Sin. **63**(7), 78704 (2014)
59. Mojtaba, M.A., Valizadeh, A., Tass, P.A.: Dendritic and axonal propagation delays determine emergent structures of neuronal networks with plastic synapses. Sci. Rep. **7**, 39682 (2017)
60. Mojtaba, M.A., Valizadeh, A., Tass, P.A.: Propagation delays determine neuronal activity and synaptic connectivity patterns emerging in plastic neuronal networks. Chaos Interdiscip. J. Nonlinear Sci. **28**(10), 106308 (2018)
61. Mojtaba, M.A., Valizadeh, A., Tass, P.A.: Delay-induced multistability and loop formation in neuronal networks with spike-timing-dependent plasticity. Sci. Rep. **8**(1), 12068 (2018)
62. Karoly, P.J., Goldenholz, D.M., Freestone, D.R., Moss, R.E., Grayden, D.B., Theodore, W.H., Cook, M.J.: Circadian and circaseptan rhythms in human epilepsy: a retrospective cohort study. Lancet Neurol. **17**(11), 977–985 (2018)
63. Loddenkemper, T., Vendrame, M., Zarowski, M., Gregas, M., Alexopoulos, A., Wyllie, E., Kothare, S.: Circadian patterns of pediatric seizures. Neurology **76**(2), 145–153 (2011)